AMERICAN SOCIETY FOR MICROBIOLOGY | mBio®

RESEARCH ARTICLE

# Stimulated Organic Carbon Cycling and Microbial Community Shift Driven by a Simulated Cold-Seep Eruption

Yongxin Lv,[a,b,c,d] Shanshan Yang,[a,c,f,g] Xiang Xiao,[b,c,d,e] Yu Zhang[a,b,d]

[a]School of Oceanography, Shanghai Jiao Tong University, Shanghai, People's Republic of China
[b]State Key of Laboratory of Ocean Engineering, Shanghai Jiao Tong University, Shanghai, People's Republic of China
[c]School of Life Sciences and Biotechnology, Shanghai Jiao Tong University, Shanghai, People's Republic of China
[d]International Center for Deep Life Investigation (IC-DLI), Shanghai Jiao Tong University, Shanghai, People's Republic of China
[e]Laboratory for Marine Biology and Biotechnology, Pilot National Laboratory for Marine Science and Technology, Qingdao, People's Republic of China
[f]College of Marine Science and Technology, China University of Geosciences, Wuhan, People's Republic of China
[g]Shenzhen Yuchi Inspection & Testing Technology Co., Ltd., Shenzhen, People's Republic of China

**ABSTRACT** Cold seeps are a major methane source in marine systems, and microbe-mediated anaerobic oxidation of methane (AOM) serves as an effective barrier for preventing methane emissions from sediment to water. However, how the periodic eruption of cold seeps drives the microbial community shift and further affects carbon cycling has been largely neglected, mainly due to the technical challenge of analyzing the *in situ* communities undergoing such geological events. Using a continuously running high-pressure bioreactor to simulate these events, we found that under the condition of simulated eruptions, the abundance of AOM-related species decreased, and some methane was oxidized to methyl compounds to feed heterotrophs. The methanogenic archaeon *Methanolobus* replaced ANME-2a as the dominant archaeal group; moreover, the levels of methylotrophic bacteria, such as *Pseudomonas*, *Halomonas*, and *Methylobacter*, quickly increased, while those of sulfate-reducing bacteria decreased. According to the genomic analysis, *Methylobacter* played an important role in incomplete methane oxidation during eruptions; this process was catalyzed by the genes *pmoABC* under anaerobic conditions when the methane pressure was high, possibly generating organic carbon. Additionally, the findings showed that methyl compounds can also be released to the environment during methanogenesis and AOM under eruption conditions when the methane pressure is high.

**IMPORTANCE** In the ocean, almost all of the emission and consumption of deeply buried methane occurs in cold seeps; therefore, understanding the methane cycling in cold seeps is crucial to estimating the oceanic methane budget. Cold-seep eruptions often lead to the dramatic destruction of microbial ecosystems that drive methane cycling. Because of technical challenges, the direct monitoring of these communities as well as the activity shifts during eruptions has never been achieved. In this study, we took an alternative approach by simulating cold-seep eruptions and using genome-resolved metagenomics to interpret the dynamic changes in the microbial community. The results show that the periodical cold-seep eruptions intensify organic carbon cycling, undermine the direct oxidation of methane to carbon dioxide, and drive microbial community shifts. These results further suggest that a more sophisticated calculation of the methane budget in cold seeps that considers their eruption status is needed.

**KEYWORDS** cold-seep microbiome, methane oxidation, methane partial pressure

Cold seeps are the areas of seepage of hydrogen sulfide, methane, and other hydrocarbon-rich fluids, which originate from tens of meters to kilometers below the seafloor (1, 2). The ecosystem here mainly depends on the anaerobic oxidation of

**Editor** María Mercedes Zambrano, Corporación CorpoGen



Address correspondence to Yu Zhang, zhang.yusjtu@sjtu.edu.cn, or Xiang Xiao, zjxiao2018@sjtu.edu.cn.

The authors declare no conflict of interest.

**Received** 13 January 2022
**Accepted** 28 January 2022
**Published** 1 March 2022

methane (AOM) acting as an energy source, together with the organic carbon input from the water column (3). *In vitro* studies suggest that anaerobic methanotrophic archaea (ANME) exhibit AOM activity and are mostly associated with sulfate-reducing bacteria (SRB), which oxidize methane to bicarbonate or acetate for utilization by heterotrophs (4–7). Moreover, AOM is an important barrier preventing methane emissions from anoxic sediments to water columns. It is estimated that up to 300 Tg of methane per year, ~88% of the methane from the subsurface, is consumed through AOM (8). This number may be underestimated since recent research has demonstrated that 3 to ~25% of methane consumed by ANME goes to acetate and thus contributes to the organic carbon pool (5). Considering that the AOM process is the only pathway to convert methane into carbon compounds that can be utilized by life in anoxic zones, the methane budget and the carbon bioavailability in anoxic cold seep sediment are directly affected by AOM (9, 10). In addition, the global distribution along active and passive margins and substance exchange among the seafloor make cold seeps important for the biogeochemical cycle (1, 11, 12).

However, most of the research has focused on stable cold seeps. Cold seeps along the active margins would exhibit many geologic activities, and the resulting eruptions would ultimately affect the ecosystem and disturb AOM activity (12). A series of studies on the Håkon Mosby Mud Volcano showed that eruptions would increase gas and fluid emissions and significantly impact faunal density, microbial activity, and environmental variables (13–15). The sediment was observed to have rapid uplift and fall caused by the expansion and release of trapped gases (15). There was a similar phenomenon in "HaiMa" cold seeps, with a larger movement scale (16). In addition, organism distribution, formation of gas hydrate, precipitation of carbonate, and generation of new fractures are also affected by gas emissions, and eruption influences gas emissions (16). In summary, the seafloor morphology, chemosynthetic taxa in cold seeps, and metabolic activities are significantly affected by natural disturbances (17). However, due to technical challenges in directly monitoring dramatically unstable environments, limited investigations have been carried out. The exact community shifts and changes in AOM activity during the eruption remain unrevealed.

In this research, we took an alternative approach using a continuously running high-pressure bioreactor to simulate cold-seep eruption. As previously described, this reactor is specifically designed to simulate the erupting environments in the deep sea, such as cold seeps and hydrothermal vents (18). It has been successfully used to sustain and to investigate the ANME/SRB community (19). Basically, in this system, we control the methane partial pressure and incubation pressure independently to simulate the gas emission and vertical lift caused by eruption. The AOM activity and the microbial community were closely monitored during the experiment. Here, we systematically illustrate the ecological impacts on AOM activity, microbial community structure, and microbial metabolism driven by cold-seep eruptions.

## RESULTS

**Dynamic changes in AOM activity along the simulated eruption.** In this study, we simulated a cold-seep eruption event to investigate its effect on the microbial community. The original sample was collected from a mud volcano in the Gulf of Cadiz that is rich in methane and contributes to the cold-seep ecosystem (19–21). The sample was first cultivated for 8 years under a condition in which methane and sulfate were supplied as the only energy sources to enrich AOM-related species. The sample was then incubated in a continuously running high-pressure bioreactor that could independently control the methane partial pressure (MPP) and incubation pressure (IP), and the highly active AOM community was enriched and used as the biomass for the following experiments (18). During the incubation, continuous flow removed the metabolic products to avoid their inhibition of AOM activity. At the same time, it prevented the toxicity of sulfide accumulation on SRB (22). Six incubations were carried out, and each lasted for 2 months. The incubation conditions are shown in Table 1 and

**TABLE 1** Experimental design showing the incubation conditions

| Stage | Incubation name | IP (MPa) | MPP (MPa) | Time (mo) |
|---|---|---|---|---|
| Pre-I | Origin | | | 96 |
| I | L8 | 8 | 8 | 2 |
| | L15 | 15 | 8 | 2 |
| | L30 | 30 | 8 | 2 |
| | L8II | 8 | 8 | 2 |
| II | H15 | 15 | 12 | 2 |
| | H30 | 30 | 12 | 2 |

Materials and Methods in detail. Briefly, there were two stages with different MPPs. In the first stage, which contained the first four incubations, the MPP was set to 8 MPa to serve as a control and identify the effect of the incubation pressure independently. The L8II incubation was set for the recovery of the microbial community, which suffered from high incubation pressure during the two previous incubations. The MPP was then elevated to 12 MPa in the second stage to simulate cold-seep eruption events. During each stage, the IP was adjusted to mimic sediment movement.

To monitor the AOM activity, the key compound concentrations were measured every 2 days, and the results showed that the AOM activity was controlled by both IP and MPP (Fig. 1a; see also Table S1 in the supplemental material). As indicated by the production of sulfide, the optimal IP was 15 MPa, which is in accordance with the original water depth (1,200 m) of the inoculum. The increased MPP, simulating the eruption, may promote this and had apparent benefit for the community to cope with high IP. For example, under 15 MPa of IP, sulfide production increased from 2.30 to 8.21 $\mu$mol per day when the MPP was increased from 8 to 12 MPa (Fig. 1a). There was no sulfide production under 30 MPa of IP (L30) when the MPP was low, but apparent activity was detected when the MPP was adjusted to 12 MPa (H30). A larger biomass observed between the same two incubations may also suggest a stronger resistance against a high IP (Fig. 1b and Table S2).

**In-depth investigation of the community composition.** Both metagenome and amplicon sequencing were performed at the end of the incubation and with the original cultivated sample (Origin). For amplicon data sets, the SILVA 138 database (23) and QIIME2 (24) were used to determine the taxonomic composition and diversity. For metagenome data sets, a genome-centric analysis was also performed to illustrate the community structure at the taxonomic level. A total of 1,766,410,042 clean reads remained after quality control and were used in the coassembly. A total of 170,472 scaffolds were obtained after sequences of $<$500 bp were filtered. More than 99% of reads could be successfully mapped to these scaffolds and resulted in a range of average sequencing depths from 50.32 to 71.79 (Table S3). A total of 110 metagenome-assembled genomes (MAGs) were reconstructed with 80 high-quality drafts (completeness $>$ 90%) and 28 medium-quality drafts (completeness between 50% and 89.9%) based on the MixS standard (25), which covers 19 phyla and nearly 80% of all reads (Fig. 2 and Table S3). ANME-2a and *Methanolobus* are the dominant archaeal groups, while *Desulfobacterota* and *Gammaproteobacteria* are the dominant bacterial members.

Moreover, 30 out of 80 high-quality drafts were identified as novel taxa with no reference genome in the Genome Taxonomy Database (GTDB) database (26). In addition to the ANME-2a MAG reported in previous research (5) (Cadiz_LYX17), another two ANME-2a MAGs were identified in this study (Cadiz_LYX29 and Cadiz_LYX78).

**Effect of IP on the microbial activity and community.** Using the continuous bioreactor, we were able to reveal the effects of the IP and MPP independently. In general, the microbial sensitivity to IP defines the water depth of their natural habitat, and the MPP defines the Gibbs free energy in the AOM reaction, which could be utilized for microbial growth. In this study, we set the IP to 8, 15, and 30 MPa to mimic the vertical migration of the active AOM community driven by the eruption. The community had the highest biomass with an IP of 15 MPa, which is similar to the pressure at its original

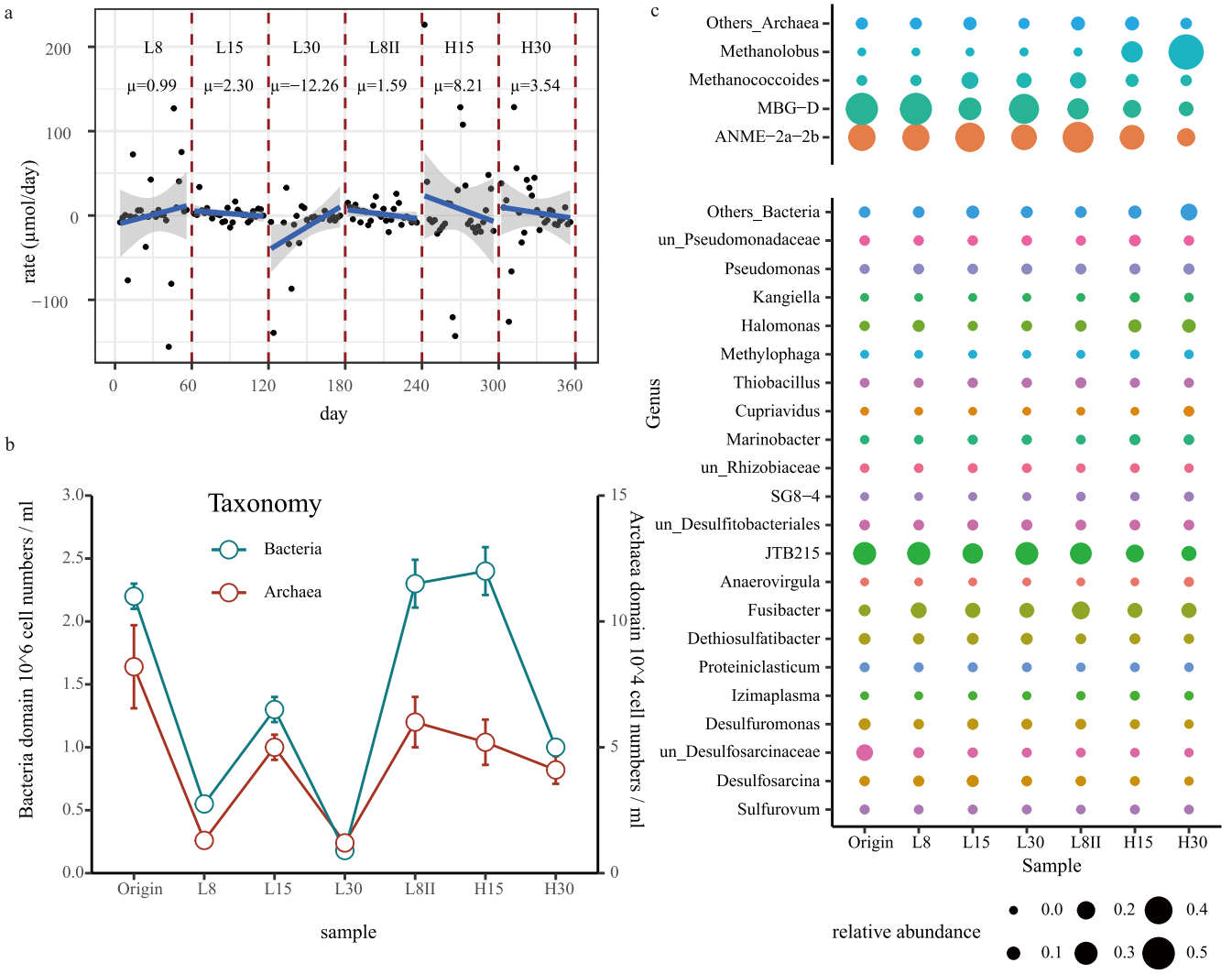


**FIG 1** Microbial activities and cellular quantifications under different incubation conditions. (a) The mean value ($\mu$) and standard deviation of sulfide production rate were calculated based on *n* values of 27 (L8), 28 (L15), 25 (L30), 28 (L8II), 28 (H15), and 28 (H30). (b) The mean value and standard deviation of archaeal and bacterial cell numbers were calculated based on an *n* value of 3. (c) Microbial community structure shift during incubation. The point size shows the relative abundance of each genus for bacteria (bottom) and archaea (top). Different colors represent the different genera, and genera whose relative abundances were <0.01 were grouped into "Others."

sampling site (1,200-m water depth), while increases in the IP to 30 MPa caused apparent decreases in biomass and AOM activity under both low and high MPP (Fig. 1a and b).

**Effect of MPP on the microbial activity and community.** MPP mostly influenced the taxonomic composition and further metabolic functions (Fig. 3). Most previously dominant species were strongly stirred under higher MPP, especially ANME-2a-2b and SRB (Fig. S1). *Methanolobus* replaced ANME-2a-2b as the dominant archaeal group under higher MPP (Fig. 1c). Bacterial groups that reduce inorganic sulfur compounds, including *Desulfobacteraceae*, *Defulfitobacteriales*, and *Desulfuromonas*, were dominant but continued to decrease over the experimental period, especially when the MPP was changed to 12 MPa. A similar trend was observed with *Clostridia* JTB215. The abundance of another abundant group, *Fusibacter*, increased when the IP was adjusted to 8 MPa both the first time (from 6.37% to 14.98%) and the second time (from 13.03% to 19.21%). In addition, the abundance of *Pseudomonas* was relatively stable (6.67% to ~11.08%). In addition, methylotrophic MAGs increased under higher MPP, such as *Pseudomonas* (Cadiz_LYX64 and Cadiz_LYX94), *Halomonas* (Cadiz_LYX97 and Cadiz_LYX58), and *Methylobacter* (Cadiz_LYX74) (27, 28), while *Firmicutes* (mainly *Clostridia*) decreased, suggesting a distinct primary energy process and the emergence of a heterotrophic community.

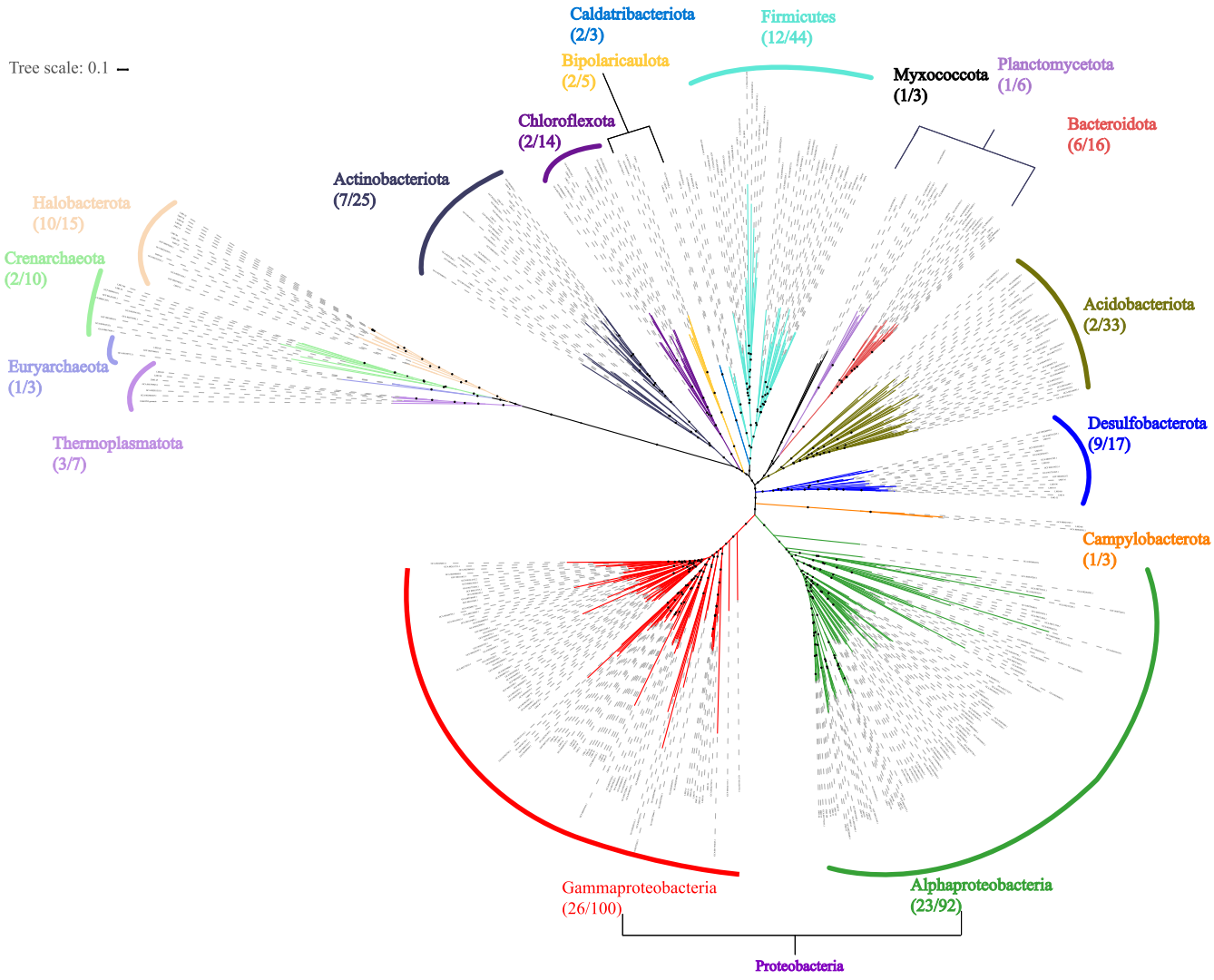


**FIG 2** Phylogenetic tree of retrieved metagenome-assembled genomes (MAGs) based on concatenated conserved proteins. A total of 40 conserved genes were used to generate a maximum likelihood tree. Bootstrap support is indicated by the size of the black dots, and those representing 70% are depicted. The numbers under the phylum names represent the numbers of retrieved MAGs in this study (left) and reference genomes (right).

To verify this finding, an analysis of the key genes and metabolic modules was performed. A custom Python script, which is similar to KEGG-Decoder (29) but expanded to more modules and functions, was used to evaluate the related metabolic ability of 30 abundant MAGs (whose difference in abundance between incubation L15 and H15 was >0.1%) (Fig. 4 and Table S3). MAG "Cadiz_LYX17," which belonged to ANME-2a and was the only abundant archaeal participant in AOM, decreased under higher MPP. This was consistent with the amplicon sequencing results. Similarly, the relative abundance of 4 out of 6 MAGs that had a complete dissimilatory sulfate reduction (DSR) pathway decreased. However, one of them belonged to *Thiobacillus* (Cadiz_LYX39), which reportedly carries out the reverse DSR (30). At the same time, although MAG Cadiz_LYX65 also belonged to *Desulfobacterota* and was mostly complete (99.32%), none of the DSR-related genes were identified. It was found that the system became more diversified in terms of metabolic potential, especially carbon flow, under the simulated erupting conditions. Larger abundances of the formaldehyde assimilation pathway (Entner-Doudoroff [EDD] pathway) and methylotrophs indicate that there would be methyl-like substances for the emerging heterotrophs to utilize (Fig. 4 and Fig. S2).

The metabolic pathways associated with sulfur in the community also became more complex. Genes related to assimilatory sulfate reduction and thiosulfate

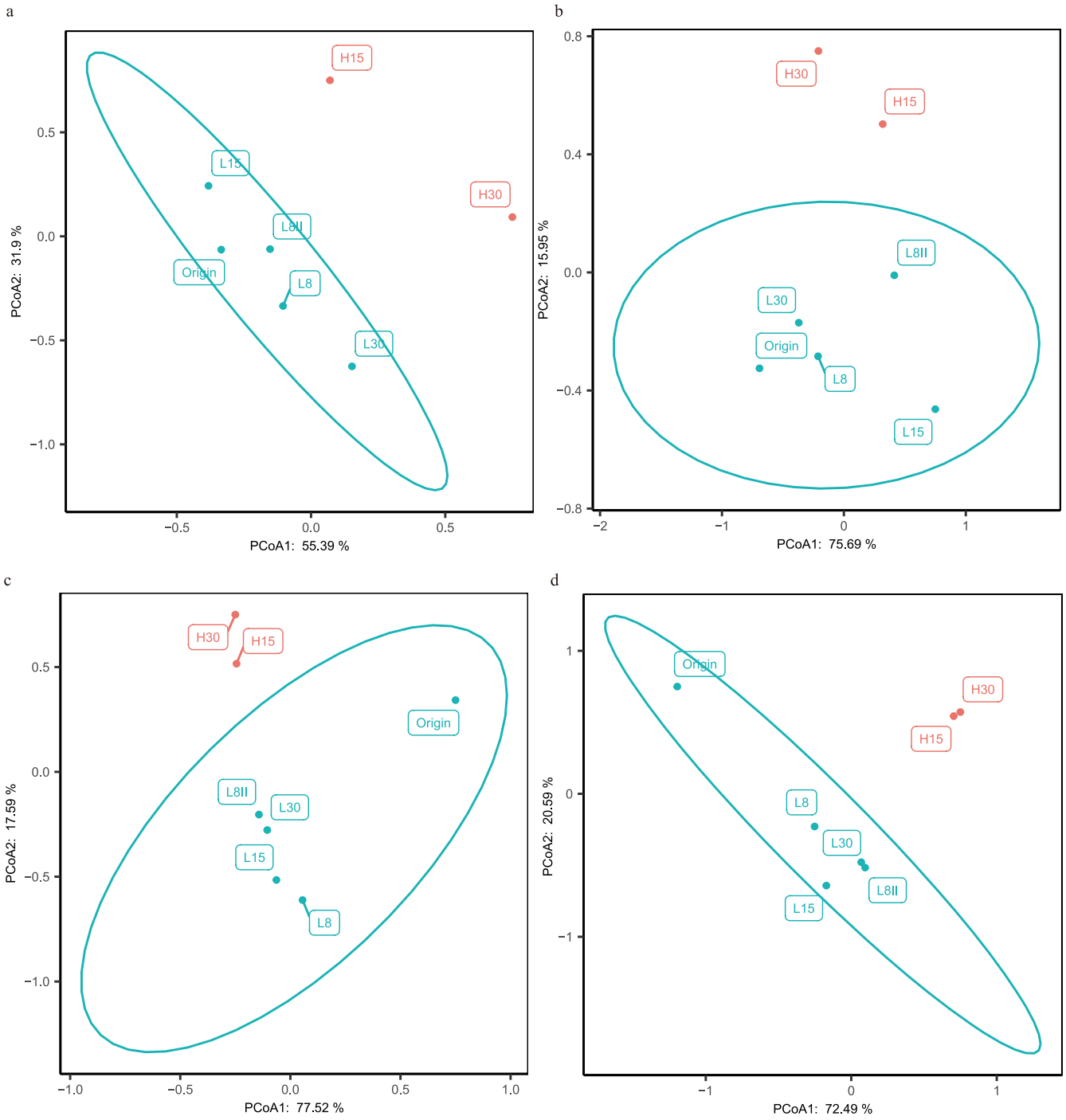


**FIG 3** Principal-component analysis (PCoA) of incubations with different conditions, as follows: Based on the read number of each archaeal amplicon sequence variant (ASV) (a), based on the read number of each bacterial ASV (b), based on the relative abundances of 43 abundant MAGs (c), and based on the relative abundances of KEGG orthologs (d).

oxidation, which mainly belonged to *Pseudomonas*_A (Cadiz_LYX64 and Cadiz_LYX94), *Cupriavidus* (Cadiz_LYX104), and *Marinobacter* (Cadiz_LYX88 and Cadiz_30), were more enriched under erupting conditions. In addition, *Cupriavidus* and *Ralstonia* (Cadiz_LYX72) also degrade alkanesulfonate and taurine to sulfite, which is then reduced to sulfide and cysteine (Fig. 4). In addition, a higher abundance of transporter genes for these three sulfur compounds also showed enhanced assimilation (Fig. S2). Combined with the enhanced assimilation, higher energy input, and biomass, the community would have a better resistance to a higher IP under erupting conditions (H30) than under nonerupting

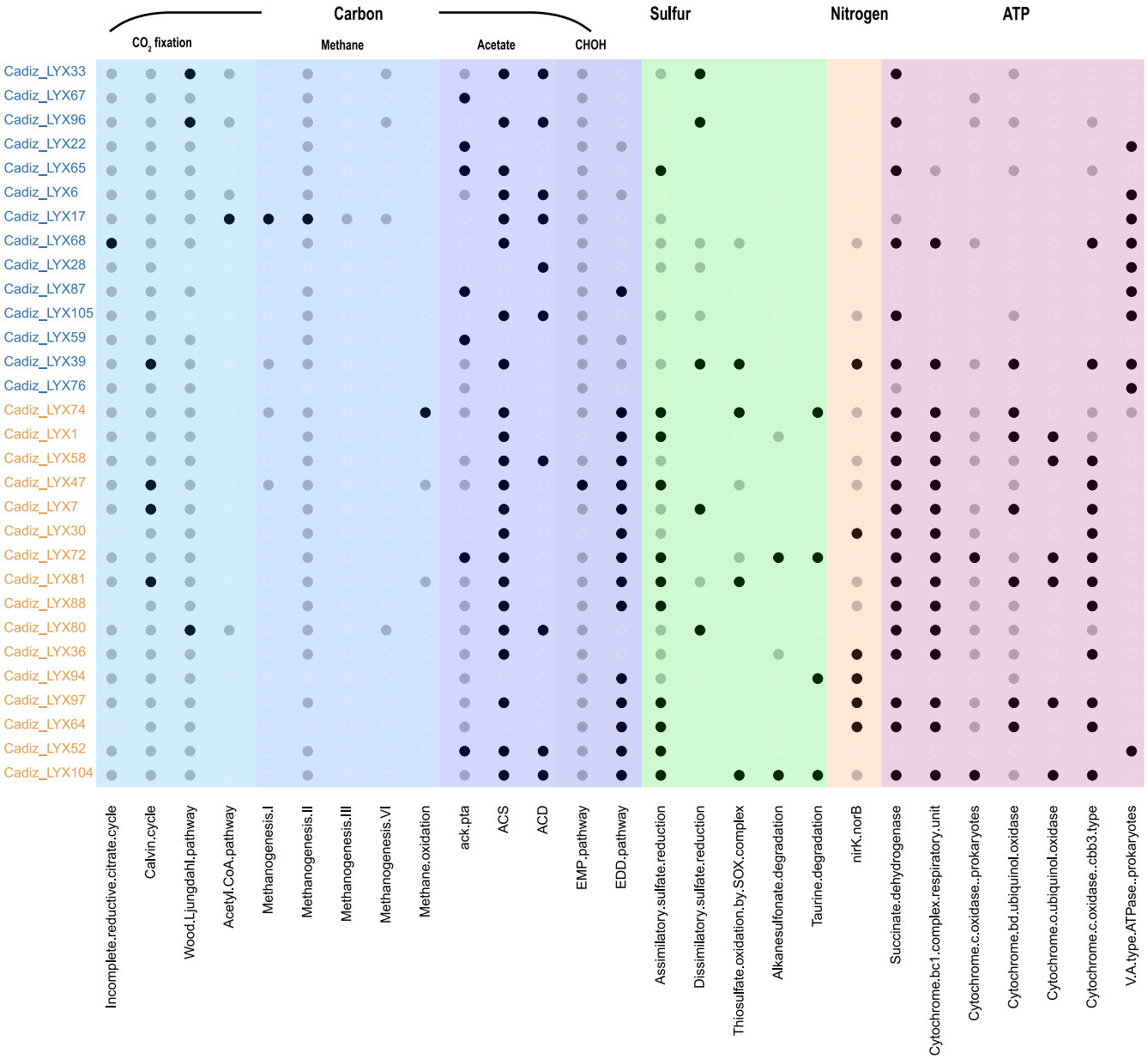


**FIG 4** Metabolic potential of 30 abundant MAGs. A black dot indicates a complete or nearly complete pathway (>0.75), a gray dot only partial gene existence (≥0.2 and <0.75), and a blank a lack of related genes (<0.2). MAGs with blue color would have a lower relative abundance in incubation H15, and MAGs with orange color would have a larger relative abundance. EMP, Embden-Meyerhof-Parnas; EDD, Entner-Doudoroff.

conditions (L30). Higher Shannon and Pielou diversity indices were also observed (Table S4), which could aid the stability of microbial communities in the face of fluctuations in environmental factors (31).

**Conceptual model of the community shift.** A conceptual model was proposed to reflect the community shift at both the taxonomic and metabolic levels (Fig. 5). Under nonerupting conditions, anaerobic oxidation of methane-sulfate reduction (AOM-SR) activity conducted by ANME-2a and SRB was the primary process. AOM-SR was used as the keystone of the system. The products carbon dioxide and acetate would be used by the heterotrophic community, which was composed mainly of *Clostridia* (46.61% to ~54.13%), followed by *Gammaproteobacteria* (14.54% to ~21.48%). Under simulated erupting conditions, this relative importance of AOM activity was inhibited, and alternative pathways were observed for both sulfate and methane consumption. In addition to ANME, a portion of methane was oxidized through *Methylobacter* (Cadiz_LYX74) and *Methanolobus*.

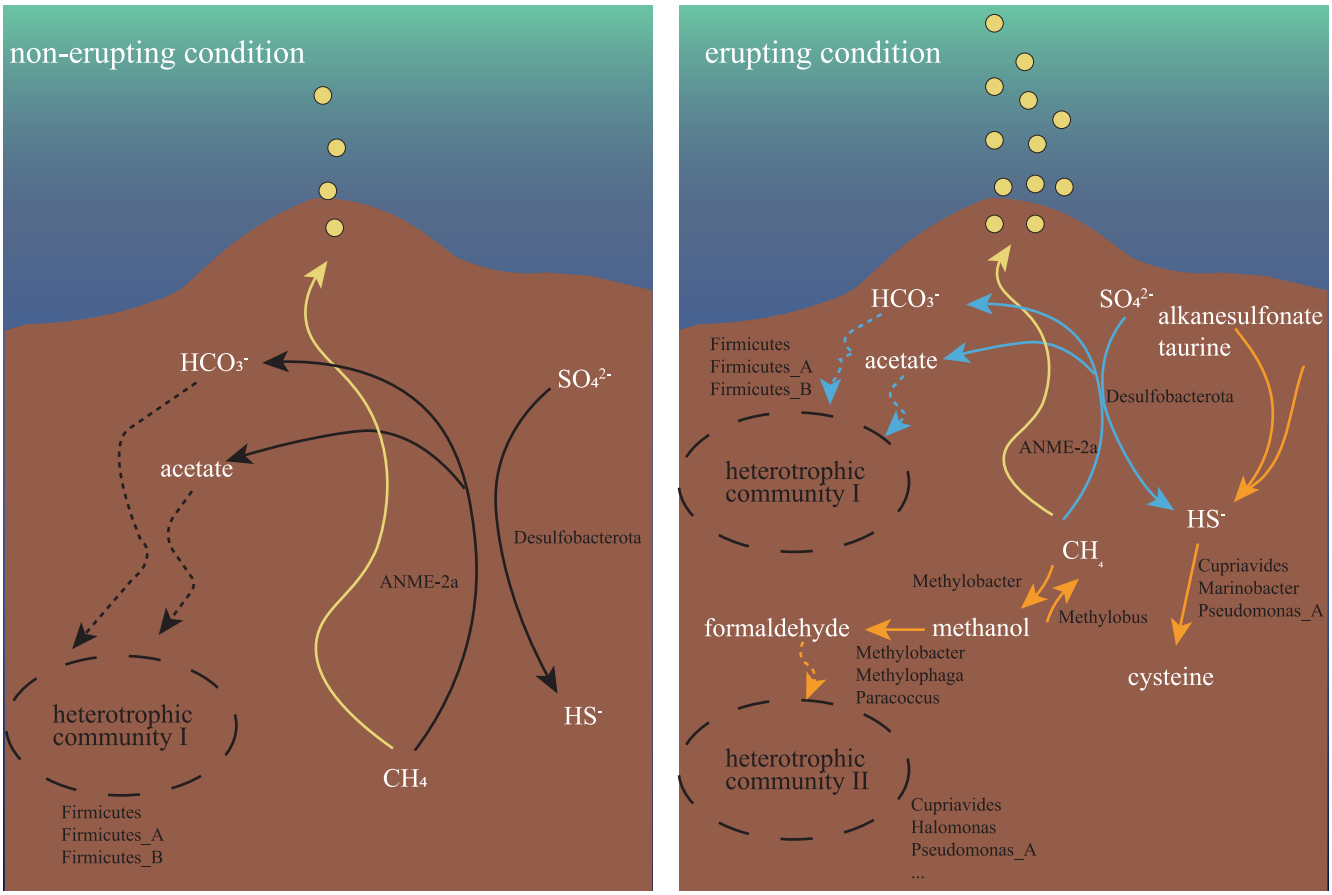


**FIG 5** Proposed conceptual model for community shift during the cold-seep eruption. Abundant taxonomy and process before the eruption (left) and during the eruption (right). Color in the right part represents the changes in abundance; blue represents a decrease and orange represents an increase.

Methylobacter (Cadiz_LYX74), *Paracoccus* (Cadiz_LYX81) and *Methylophaga* (Cadiz_LYX47), oxidize the product methanol to formaldehyde, which is then assimilated by the emerging heterotrophic community consisting of *Gammaproteobacteria*. Sulfate was transported into cells and assimilatorily reduced to sulfide, alkanesulfonate, and taurine. Above all, a more complex metabolic network was observed.

## DISCUSSION

In this study, by simulating a cold-seep eruption with a continuously running high-pressure bioreactor, the cold-seep microbial community was found to be sensitive to IP and MPP, with the former mainly influencing the biomass. Generally, higher IP would cause major damage to cells and decrease biomass, but this was not the case when it was adjusted to 15 MPa. This result may be caused by the large decrease in ANME-2a, as it was regarded as the sole group to provide energy through the oxidation of methane. The preference of ANME-2a in a certain pressure range has been confirmed by cultivation-based experiments as well as omics-based investigations, and this finding is in accordance with the water depth range of their distribution in nature (32–34). In general, high incubation pressures cause intracellular oxidative stress (35–37). Since this community was incubated under high pressure for years, the dominant groups are piezotolerant and piezophilic and have thus developed strategies to cope with oxidative stress. For example, ANME-2a has genes for cytochrome *c* and membrane-associated coenzyme B-coenzyme M heterodisulfide reductase (HdrDE) in its electron transfer system, and this strain is often found in environments with oxygen intrusion (38, 39). Interestingly, as suggested by our results, the damaging effect of high IP was reversible. After IP was changed to 8 MPa again (L8II), the community seemed to recover

from the disturbance. First, the biomass of ANME-2a and SRB increased as much as that of L15 (Fig. S1), and ANME-2a became the dominant archaeal group (Fig. 1b). In addition, positive sulfide production was observed, suggesting that during this incubation, the community was based on AOM-SR activity. Similar taxonomic compositions (Fig. 3) also suggested recovery.

MPP mostly influenced the taxonomic composition and metabolic function (Fig. 3). Under higher MPP, some methane may also be converted to methyl-like substances for emerging heterotrophs to utilize. Though commonly regarded as a reaction for which oxygen is required, this process was demonstrated to occur in anoxic environments (40). Since the high pressure induces the intracellular production of reactive oxygen species, this methyl production process may be more feasible under eruption conditions (35). We consider two sources of methyl-like substances.

**(i) Methane oxidized to methanol by the enzyme PmoABC and further to formaldehyde.** Although regarded as an aerobic reaction, the process from methane to methanol has been observed and reported for several natural anoxic environments and anaerobic incubation conditions (40–46). Most reported methane oxidizers are *Methylobacter*, utilizing nitrate or nitrite to catalyze the conversion from methane to methanol and finally to formaldehyde for utilization. Although there were relatively low concentrations of nitrate and nitrite, this low concentration could lighten the toxic effect of the reduced product, NO. At the same time, *Methylobacter* was reported to perform high-rate methane oxidation in the anoxic hypolimnion stimulated by both sulfate additions (40). An emerging MAG, Cadiz_LYX74, also belongs to the same genus and possesses the same functional gene sets for denitrification (*nirK* and *norB*) and methane oxidation (*pmoABC*), giving the possibility of "aerobic" methane oxidation. The latter also was found to be present and transcribed in the anoxic environment (43, 47, 48). A recent study by He et al. also showed that aerobic gammaproteobacterial methanotrophs dominated in the assimilation of $CH_4$, both in their DNA-based stable isotope probing incubations and in the active methane seep (anaerobic region, down to 70 cm deep in sediments) (49). Additionally, the metagenomic result of the heavy DNA showed that *Methylobacter* (27.0%) was the most abundant gammaproteobacterial methanotroph, which was consistent with our results. Moreover, the genes *pmoABC* in the MAG Cadiz_LYX74 were also found to be expressed (with transcripts per kilobase million [TPM] values of 88.99, 94.24, and 1213.12, respectively) in the metatranscriptomic reads collected from the incubation in the same continuous high-pressure bioreactor for 1 year (38).

**(ii) Leakage from activated ANME.** Methanogenesis was observed in three AOM enrichment cultures by Wegener and coworkers. Further enrichments with different substrates suggested that the methane came from methanol and methylamine instead of hydrogen, acetate, and carbon monoxide (50). Those methyl-like substances were proposed as intermediates from methyl-S-CoM (51) in ANME-1, with the absence of the methylenetetrahydromethanopterin reductase (Mer) enzyme from a strict reversal of methanogenesis. A high methane partial pressure would increase the amount of methyl-S-CoM and further stimulate methylated production.

Additionally, 14 out of 16 MAGs that exhibited increasing abundance belonged to the EDD pathway, which could assimilate formaldehyde. Considering the decreasing abundance of genes related to carbon dioxide fixation (Fig. S2) and the decrease in ANME-2a and SRB (Fig. S1), it was proposed that methylated compounds may act as alternative substrates to support the emerging community. Although previous studies showed that a higher MPP would promote AOM activity (19, 52–55), the highest MPP was set to 10 MPa. Shallow marine sediment was incubated at different pressures (pressurized with 100% $CH_4$) by Cassarini et al., and there was also a lower sulfide production and AOM rate under higher MPP (20 and 40 MPa) than lower MPP (0.1, 0.45, and 10 MPa), suggesting substrate inhibition during AOM activity (56). The production of methanol also stimulated the emergence of *Methanolobus* (Cadiz_LYX86), whose biomass and abundance increased under eruption conditions (Fig. S1 and Table S3). At the same time, the methanol that was produced could serve as the methanogenic

substrate for *Methanolobus*. Methanol was a noncompetitive substrate for methanogens and sulfate reducers (or other heterotrophs), which was observed previously in cold-seep sediments (57, 58). Additionally, a higher methanogenesis rate was observed in the incubation of site GC600 under higher MPP (25 mM methane) than under lower MPP (5 mM methane) (59). The importance of methanol-related methanogenesis has been suggested in both *in situ* and *in vitro* investigations.

**Conclusions.** In conclusion, by enriching the AOM-SR-related microbiome and simulating cold-seep eruption events, we revealed the community drift caused by higher MPP. During geological activities, the community became more diverse, in terms of both taxonomy composition and metabolic potential. AOM-SR activity and the related species were not the exclusive keystones of the cold-seep community, and methane was utilized by multiple pathways, such as oxidation and subsequent formaldehyde assimilation. An unexpected and complex microbial community was revealed under high MPP; in this community, canonic AOM-SR activity was suppressed, and organic carbon production was stimulated. This diversity in taxonomy and metabolic potential would better maintain community stability. In other words, environmental conditions drive the generation of microdiversity (31). These findings emphasize the enormous ecological impact of methane eruptions on cold-seep ecosystems. As a result, more sophisticated *in situ* measurements and modeling of the methane budget in cold seeps that consider AOM-SR suppression by higher MPP and organic carbon derived from incomplete AOM are needed.

## MATERIALS AND METHODS

**Sample site, continuous high-pressure incubation, and activity analysis.** The inoculum was originally obtained from Captain Arutyunov Mud Volcano (35° 39.700′N; 07° 20.012′W) at 1,200 m below the seafloor and had been incubated in a continuous high-pressure bioreactor for 8 years (incubation origin) (19, 60). In this study, six other incubations with different combinations of MPP and IP were carried out (Table 1). Based on the calculated methane affinity for the same ANME-2/SRB community, 8 MPa of methane was provided in the first 4 incubations to achieve the maximum AOM rate (61). The MPP was then adjusted to 12 MPa to mimic a cold-seep eruption. The IP was set to 8 MPa, 15 MPa, and 30 MPa for the simulation of cold seeps at different depths. Every liter of medium consisted of the following: NaCl at 26 g, $MgCl_2 \cdot 6H_2O$ at 5 g, $CaCl_2 \cdot 2H_2O$ at 1.4 g, $Na_2SO_4$ at 1.3 g, $NH_4Cl$ at 0.3 g, $KH_2PO_4$ at 0.1 g, KCl at 0.5 g, bicarbonate solution at 30 mL, vitamin mixture solution at 1 mL, trace element solution at 1 mL, thiamine solution at 1 mL, and vitamin $B_{12}$ solution at 1 mL. The bicarbonate solution, vitamin solutions, and trace element solution were prepared according to the method of Widdel and Bak (62). The pH of the medium was adjusted to 6.8 by adding sulfuric acid. The medium was prepared under a nitrogen atmosphere; it was first saturated with high-pressure methane and then transferred to the bioreactor at a flow rate of 0.1 mL/min. Incubation was performed at 15°C, and the methane pressure and incubation pressure were changed every 2 months. To monitor AOM-SR activity, the consumption of methane and sulfate, as well as the production of carbon dioxide and sulfide, was analyzed as previously described (63). Of these 4 methods, the quantification of sulfide is the most sensitive for determining AOM activity. All of the sulfide produced comes from sulfate reduction using methane or intermediates derived from methane oxidation as the electron donor. Moreover, there was no sulfide pool in the inlet, so the sulfide production could be precisely quantified. Since we were running a flowthrough system, the sulfide production rate was calculated by measuring the sulfide concentrations from the inlet and outlet of the incubation vessel and considering the incubation volume and flow rate. For acetate measurement, 1 mL of sample filtered through a 0.22-$\mu$m membrane filter (Merck Millipore, Billerica, MA) was mixed with 0.25 mL of 50% $H_2SO_4$, and 1 mL of ether solution containing internal standard 2-methylpentanoic acid (50 $\mu$g/ml) was then added. Then, the sample was centrifuged at 3,000 rpm for 10 min at 4°C and incubated at 4°C for 30 min. The top layer was injected into a gas chromatograph–triple-quadrupole mass spectrometer (GC-QQQ-MS; Agilent 7890B-7000D; Agilent Technologies, Santa Clara, CA). The detection limit was lower than 80 nM.

**Analysis of 16S rRNA sequencing data.** DNA was extracted and purified according to the modified SDS-based method described by Natarajan et al. (64). Purified DNA was dissolved in 60 $\mu$L of double-distilled water ($ddH_2O$) and stored at −80°C until use. The V4 region of bacterial 16S rRNA genes was amplified by PCR with the primer pair Bact533F (5′-TGCCAGCAGCCGCGGTAA-3′) and Bact806R (5′-GGACTACCAGGGTATCTAATCCTGTT-3′), while the V4-V5 region of archaeal 16S rRNA genes was amplified with the primer pair Arch516F (5′-TGYCAGCCGCCGCGGTAAHACCVGC-3′) and Arch855R (5′-TCCCCCGCCAATTCCTTTAA-3′) (65). The 50-$\mu$L amplification mixture contained 1 $\mu$L of each forward and reverse primer, 1 $\mu$L of template DNA, 5 $\mu$L of 10× *Ex Taq* buffer, 5 $\mu$L of 2.5 mM deoxynucleoside triphosphate (dNTP) mix, 0.25 $\mu$L of *Ex Taq* polymerase (TaKaRa, Tokyo, Japan) and 39.75 $\mu$L of $ddH_2O$. The PCR conditions for archaeal 16S rRNA gene amplification were as follows: 94°C for 5 min, followed by 35 cycles at 94°C for 40 s, 60°C for 40 s, and 72°C for 50 s and a final extension at 72°C for 10 min. For bacteria, the PCR conditions were 94°C for 5 min, 25 cycles of 40 s at 94°C, 40 s at 58°C,

and 30 s at 72°C, and a final extension for 10 min at 72°C. The PCR products were purified with an E.Z.N.A. gel extraction kit (Omega Bio-Tek, Norcross, GA). The 16S rRNA gene amplicons containing the unique barcodes used for each sample were pooled at equal concentrations and sequenced on an Illumina MiSeq platform using 2 × 250-bp cycles at Shanghai Personal Biotechnology Co., Ltd. (Shanghai, China). The raw sequence reads were quality filtered using an average quality value of 20 during demultiplexing; sequences with a mean quality score of <20, a length <150 bp, or any ambiguities were excluded from the analysis. Raw tags were then generated by merging paired-end (PE) reads with FLASH (version 1.2.7) (66). The resulting sequences were imported to QIIME2 for taxonomic identification. First, the sequences of the corresponding regions from the SILVA 138 database (23) were extracted according to the primers used, and the sequences were then used to train the classifier. Then, chimeric sequences obtained during the PCR process were removed using "qiime vsearch." The taxonomy of the obtained cluster was determined by "feature classifier" with the classifier. Then, the conflicting sequences for bacteria and archaea were removed.

**Population quantification.** The bacterial and archaeal populations were quantified by quantitative PCR (qPCR). qPCR amplification was performed using a StepOnePlus real-time PCR system (Applied Biosystems, Foster, CA), and all reactions for the bacterial 16S rRNA gene were conducted using SYBR premix *Ex Taq* (TaKaRa, Tokyo, Japan). The primer pair bac331F (5′-TCCTACGGGAGGCAGCAGT-3′) and prokaryotic 797R (5′-GGACTACCAGGGTATCTAATCCTGTT-3′) was used for bacteria, and Uni519F (5′-GCMGCCGCGGTAA-3′) and Arc908R (5′-CCCGCCAATTCCTTTAAGTT-3′) (67) were used for archaea. Each reaction was conducted in triplicate. The qPCR program for bacteria was 50°C for 2 min, 95°C for 2 min, and 40 cycles of 95°C for 15 s and 65°C for 60 s. For archaea, the program was 95°C for 15 min followed by 35 cycles of 95°C for 30 s, 60°C for 30 s, and 72°C for 30 s. The quantification standard consisted of a dilution series (between $1 \times 10^3$ and $1 \times 10^9$ copies/$\mu$L) of a known amount of purified PCR product obtained from sediment environmental DNA. The $R^2$ value for the standard curve was 0.99, and the amplification efficiency was 95 to 105%. The bacterial cell number was calculated using the bacterial 16S rRNA gene copy number divided by 4, which is the mean 16S rRNA operon number for each incubation calculated by PICRUSt (Phylogenetic Investigation of Communities by Reconstruction of Unobserved States) (68). The cell numbers of ANME-2a, SRB, and *Methanolobus* were calculated using the total archaeal cell number multiplied by the relative abundance in the corresponding community.

**Metagenomic assembly, binning, and annotation.** The 150-bp paired-end raw reads of 7 incubations were first trimmed by BBDuk tools (https://sourceforge.net/projects/bbmap/) with a sequence quality score > 20 and a final minimum length of >90 bp. Then, the reads containing rare kmers (kmer depth ≤ 2) were discarded by tadpole.sh with "tossdepth = 2 ecc=t tossjunk=t mbb = 2." Next, all reads were merged into SPAdes (69) for coassembly with "--meta --only assembler -k 65,75,96,115,127." The assembly was filtered for a minimum length of >500 bp using a custom Python script. Then, reads from each incubation were mapped to the filtered assembly separately by BBMap with "k = 13 minid = 0.95 pairlen = 350 rescccuedist = 650." The mapped file in SAM format was converted to BAM format and sorted by SAMtools (70). The depth of each scaffold in every incubation was determined by the script "jgi_summarize_bam_contig_depths" from MetaBAT2 (71) with the default parameters. Three binning software programs were used to obtain the primary MAG via the depth matrix. For MetaBAT2, different sensitivities (--maxP 60, 75, and 90) and specificities (--minS 60, 75, and 90) were combined. The two marker gene sets (40 and 107) were analyzed by MaxBin (version 2.2.6) (72). CONCOCT analysis (73) was also carried out. Then DAStools (74) was used to integrate the results to calculate an optimized, nonredundant set of MAGs. Quality and taxonomy were determined by CheckM (75) and GTDBtk tools (76) with the GTDB (version r95) (26), respectively. Genes were predicted by Prodigal (77) for the filtered assembly, and those with lengths smaller than 100 bp were discarded. The modified gene set was functionally annotated with an integrated result, with the following priorities: GhostKOALA (78) > emapper (version 2.0.1) against the EggNOG database (version 5) (79, 80) > KofamKOALA (81) (version 1.0.3). FeatureCounts (82) was used to count the read number of each gene, and the TPM value was calculated with a custom Python script.

**Phylogenetic tree construction.** For the tree of MAGs, we randomly chose 1 genome as a reference for each class of the phylum occurring in the MAG taxonomic results in the GTDB. The gene of each reference genome was predicted by Prodigal. Then, fetchMG (83) was used to extract the marker gene for all MAGs and the reference genome. Then, for each marker gene set, alignment and trimming with the same parameter were performed separately by MAFFT-linsi (84) and trimAL (85) with the automated1 model. After that, all alignments were concatenated for each genome. The trimmed alignment was composed of 397 sequences and 8,836 columns. IQTREE (86) was used to construct the phylogenetic tree with the model "LG+I+G4."

**Community composition and metabolic potential analysis.** Shifts in community composition were analyzed using the ade4 R package based on the read number of archaeal and bacterial genera, the relative abundance of 43 abundant MAGs (relative abundance in any one incubation > 0.5%), and the relative abundance of KEGG orthologs. The result was visualized with the ggplot2 R package.

Statistical analyses of key genes involved in carbon, sulfur, nitrogen, and ATP metabolism between incubations L15 and H15 were performed by pairwise comparisons of their abundances using two-sided Fisher's exact test with confidence intervals at 95% significance and the Newcombe-Wilson method and Benjamini-Hochberg false-discovery rate (FDR) multiple-test correction in STAMP (87). Only the module with corrected $q$ value of <0.05 was shown.

For each MAG, the metabolic potential was evaluated by the completeness of every module, which was determined by the presence/absence of KO terms with a custom Python script. The score was

modified by the following criterion: (0.75, 1) was adjusted to 1, (0.2, 0.75) was adjusted to 0.5, and (0, 0.2) was adjusted to 0.

**Metatranscriptome sequencing and mapping.** All metatranscriptomic reads were first filtered by BBDuk tools and then aligned to a combined rRNA database from SILVA and Rfam (88) using Bowtie2 (89). The unaligned mRNA reads were mapped to the assembled scaffolds. The expression of each gene was calculated as described above.

**Data availability.** The 16S rRNA gene amplicon sequencing data and metagenomic sequencing data have been deposited in the NODE database (https://www.biosino.org/node/) under project OEP001382. All metagenome-assembled genomes have been deposited in eLMSG (eLibrary of Microbial Systematics and Genomics [https://www.biosino.org/elmsg/index]) under accession numbers LMSG_G000000632.1 to LMSG_G000000741.1.

## SUPPLEMENTAL MATERIAL

Supplemental material is available online only.

**FIG S1**, PDF file, 0.01 MB.

**FIG S2**, PDF file, 0.4 MB.

**TABLE S1**, XLSX file, 0.02 MB.

**TABLE S2**, XLSX file, 0.02 MB.

**TABLE S3**, XLSX file, 0.1 MB.

**TABLE S4**, XLSX file, 0.1 MB.

## ACKNOWLEDGMENTS

This work was supported by the National Natural Science Foundation of China (grant no. 41776173, 91951117, 41921006, 42122043, and 41476123) and National Key Research and Development Program of China (2016YFC0300709).

Y.L., S.Y., X.X., and Y.Z. designed the research. Y.L., S.Y., and Y.Z. performed the research and analyzed the data. Y.L. and Y.Z. drafted the manuscript.

## REFERENCES

1. Boetius A, Wenzhofer F. 2013. Seafloor oxygen consumption fuelled by methane from cold seeps. Nat Geosci 6:725–734. https://doi.org/10.1038/ngeo1926.
2. Vossmeyer A, Deusner C, Kato C, Inagaki F, Ferdelman T. 2012. Substrate-specific pressure-dependence of microbial sulfate reduction in deep-sea cold seep sediments of the Japan Trench. Front Microbiol 3:253. https://doi.org/10.3389/fmicb.2012.00253.
3. Coffin RB, Smith JP, Yoza B, Boyd TJ, Montgomery MT. 2017. Spatial variation in sediment organic carbon distribution across the Alaskan Beaufort Sea shelf. Energies 10:1265. https://doi.org/10.3390/en10091265.
4. Bhattarai S, Cassarini C, Lens PNL. 2019. Physiology and distribution of archaeal methanotrophs that couple anaerobic oxidation of methane with sulfate reduction. Microbiol Mol Biol Rev 83:e00074-18. https://doi.org/10.1128/MMBR.00074-18.
5. Yang S, Lv Y, Liu X, Wang Y, Fan Q, Yang Z, Boon N, Wang F, Xiao X, Zhang Y. 2020. Genomic and enzymatic evidence of acetogenesis by anaerobic methanotrophic archaea. Nat Commun 11:3941. https://doi.org/10.1038/s41467-020-17860-8.
6. Hinrichs KU, Hayes JM, Sylva SP, Brewer PG, DeLong EF. 1999. Methane-consuming archaebacteria in marine sediments. Nature 398:802–805. https://doi.org/10.1038/19751.
7. Boetius A, Ravenschlag K, Schubert CJ, Rickert D, Widdel F, Gieseke A, Amann R, Jorgensen BB, Witte U, Pfannkuche O. 2000. A marine microbial consortium apparently mediating anaerobic oxidation of methane. Nature 407:623–626. https://doi.org/10.1038/35036572.
8. Reeburgh WS. 2007. Oceanic methane biogeochemistry. Chem Rev 107:486–513. https://doi.org/10.1021/cr050362v.
9. Hu T, Luo M, Xu Y, Gong S, Chen D. 2 December 2021. Production of labile protein-like dissolved organic carbon associated with anaerobic methane oxidization in the Haima cold seeps, South China Sea. Front Mar Sci https://doi.org/10.3389/fmars.2021.797084.
10. Michaelis W, Seifert R, Nauhaus K, Treude T, Thiel V, Blumenberg M, Knittel K, Gieseke A, Peterknecht K, Pape T, Boetius A, Amann R, Jørgensen BB, Widdel F, Peckmann J, Pimenov NV, Gulin MB. 2002. Microbial reefs in the Black Sea fueled by anaerobic oxidation of methane. Science 297:1013–1015. https://doi.org/10.1126/science.1072502.
11. Chakraborty A, Ruff SE, Dong X, Ellefson ED, Li C, Brooks JM, McBee J, Bernard BB, Hubert CRJ. 2020. Hydrocarbon seepage in the deep seabed links subsurface and seafloor biospheres. Proc Natl Acad Sci U S A 117:11029–11037. https://doi.org/10.1073/pnas.2002289117.
12. Suess E. 2014. Marine cold seeps and their manifestations: geological control, biogeochemical criteria and environmental conditions. Int J Earth Sci 103:1889–1916. https://doi.org/10.1007/s00531-014-1010-0.
13. Girard F, Sarrazin J, Olu K. 2020. Impacts of an eruption on cold-seep microbial and faunal dynamics at a mud volcano. Front Mar Sci https://doi.org/10.3389/fmars.2020.00241.
14. Ruff SE, Felden J, Gruber-Vodicka HR, Marcon Y, Knittel K, Ramette A, Boetius A. 2019. In situ development of a methanotrophic microbiome in deep-sea sediments. ISME J 13:197–213. https://doi.org/10.1038/s41396-018-0263-1.
15. Feseker T, Boetius A, Wenzhofer F, Blandin J, Olu K, Yoerger DR, Camilli R, German CR, de Beer D. 2014. Eruption of a deep-sea mud volcano triggers rapid sediment movement. Nat Commun 5:5385. https://doi.org/10.1038/ncomms6385.
16. Wei JG, Li JW, Wu TT, Zhang W, Li JT, Wang JL, Tao J, Chen ZH, Wu ZJ, Chen WL. 2020. Geologically controlled intermittent gas eruption and its impact on bottom water temperature and chemosynthetic communities—a case study in the "HaiMa" cold seeps, South China Sea. Geol J 55:6066–6078. https://doi.org/10.1002/gj.3780.
17. Nakajima R, Chen C, Iwase R, Yamamoto H, Fujikura K. 2019. Clams after storms: the impact of multiple disturbances on seep vesicomyid clams revealed by long-term monitoring. Mar Biol 166:35. https://doi.org/10.1007/s00227-019-3484-6.
18. Zhang Y, Li X, Bartlett DH, Xiao X. 2015. Current developments in marine microbiology: high-pressure biotechnology and the genetic engineering of piezophiles. Curr Opin Biotechnol 33:157–164. https://doi.org/10.1016/j.copbio.2015.02.013.
19. Zhang Y, Henriet J-P, Bursens J, Boon N. 2010. Stimulation of in vitro anaerobic oxidation of methane rate in a continuous high-pressure bioreactor. Bioresour Technol 101:3132–3138. https://doi.org/10.1016/j.biortech.2009.11.103.
20. Olu-Le Roy K, Sibuet M, Fiala-Médioni A, Gofas S, Salas C, Mariotti A, Foucher J-P, Woodside J. 2004. Cold seep communities in the deep

eastern Mediterranean Sea: composition, symbiosis and spatial distribution on mud volcanoes. Deep Sea Res I Oceanogr Res Papers 51:1915–1936. https://doi.org/10.1016/j.dsr.2004.07.004.
21. Olu K, Lance S, Sibuet M, Henry P, Fiala-Médioni A, Dinet A. 1997. Cold seep communities as indicators of fluid expulsion patterns through mud volcanoes seaward of the Barbados accretionary prism. Deep Sea Res I Oceanogr Res Papers 44:811–841. https://doi.org/10.1016/S0967-0637(96)00123-9.
22. Rabus R, Heider J. 1998. Initial reactions of anaerobic metabolism of alkylbenzenes in denitrifying and sulfate-reducing bacteria. Arch Microbiol 170:377–384. https://doi.org/10.1007/s002030050656.
23. Glockner FO, Yilmaz P, Quast C, Gerken J, Beccati A, Ciuprina A, Bruns G, Yarza P, Peplies J, Westram R, Ludwig W. 2017. 25 years of serving the community with ribosomal RNA gene reference databases and tools. J Biotechnol 261:169–176. https://doi.org/10.1016/j.jbiotec.2017.06.1198.
24. Estaki M, Jiang L, Bokulich NA, McDonald D, González A, Kosciolek T, Martino C, Zhu Q, Birmingham A, Vázquez-Baeza Y, Dillon MR, Bolyen E, Caporaso JG, Knight R. 2020. QIIME 2 enables comprehensive end-to-end analysis of diverse microbiome data and comparative studies with publicly available data. Curr Protoc Bioinformatics 70:e100. https://doi.org/10.1002/cpbi.100.
25. Field D, Garrity G, Gray T, Morrison N, Selengut J, Sterk P, Tatusova T, Thomson N, Allen MJ, Angiuoli SV, Ashburner M, Axelrod N, Baldauf S, Ballard S, Boore J, Cochrane G, Cole J, Dawyndt P, De Vos P, DePamphilis C, Edwards R, Faruque N, Feldman R, Gilbert J, Gilna P, Glockner FO, Goldstein P, Guralnick R, Haft D, Hancock D, Hermjakob H, Hertz-Fowler C, Hugenholtz P, Joint I, Kagan L, Kane M, Kennedy J, Kowalchuk G, Kottmann R, Kolker E, Kravitz S, Kyrpides N, Leebens-Mack J, Lewis SE, Li K, Lister AL, Lord P, Maltsev N, Markowitz V, Martiny J, et al. 2008. The minimum information about a genome sequence (MIGS) specification. Nat Biotechnol 26:541–547. https://doi.org/10.1038/nbt1360.
26. Parks DH, Chuvochina M, Chaumeil PA, Rinke C, Mussig AJ, Hugenholtz P. 2020. A complete domain-to-species taxonomy for Bacteria and Archaea. Nat Biotechnol 38:1079–1086. https://doi.org/10.1038/s41587-020-0501-8.
27. Antony CP, Kumaresan D, Ferrando L, Boden R, Moussard H, Scavino AF, Shouche YS, Murrell JC. 2010. Active methylotrophs in the sediments of Lonar Lake, a saline and alkaline ecosystem formed by meteor impact. ISME J 4:1470–1480. https://doi.org/10.1038/ismej.2010.70.
28. Chistoserdova L, Kalyuzhnaya MG, Lidstrom ME. 2009. The expanding world of methylotrophic metabolism. Annu Rev Microbiol 63:477–499. https://doi.org/10.1146/annurev.micro.091208.073600.
29. Graham ED, Heidelberg JF, Tully BJ. 2018. Potential for primary productivity in a globally-distributed bacterial phototroph. ISME J 12:1861–1866. https://doi.org/10.1038/s41396-018-0091-3.
30. Loy A, Duller S, Baranyi C, Mussmann M, Ott J, Sharon I, Béjà O, Le Paslier D, Dahl C, Wagner M. 2009. Reverse dissimilatory sulfite reductase as phylogenetic marker for a subgroup of sulfur-oxidizing prokaryotes. Environ Microbiol 11:289–299. https://doi.org/10.1111/j.1462-2920.2008.01760.x.
31. Garcia-Garcia N, Tamames J, Linz AM, Pedros-Alio C, Puente-Sanchez F. 2019. Microdiversity ensures the maintenance of functional microbial communities under changing environmental conditions. ISME J 13:2969–2983. https://doi.org/10.1038/s41396-019-0487-8.
32. Blumenberg M, Seifert R, Reitner J, Pape T, Michaelis W. 2004. Membrane lipid patterns typify distinct anaerobic methanotrophic consortia. Proc Natl Acad Sci U S A 101:11111–11116. https://doi.org/10.1073/pnas.0401188101.
33. Thiel V, Peckmann J, Richnow HH, Luth U, Reitner J, Michaelis W. 2001. Molecular signals for anaerobic methane oxidation in Black Sea seep carbonates and a microbial mat. Mar Chem 73:97–112. https://doi.org/10.1016/S0304-4203(00)00099-2.
34. Reitner J, Peckmann J, Reimer A, Schumann G, Thiel V. 2005. Methane-derived carbonate build-ups and associated microbial communities at cold seeps on the lower Crimean shelf (Black Sea). Facies 51:66–79. https://doi.org/10.1007/s10347-005-0059-4.
35. Xiao X, Zhang Y, Wang F. 2021. Hydrostatic pressure is the universal key driver of microbial evolution in the deep ocean and beyond. Environ Microbiol Rep 13:68–72. https://doi.org/10.1111/1758-2229.12915.
36. Xie Z, Jian H, Jin Z, Xiao X. 2018. Enhancing the adaptability of the deep-sea bacterium Shewanella piezotolerans WP3 to high pressure and low temperature by experimental evolution under $H_2O_2$ stress. Appl Environ Microbiol 84:e02342-17. https://doi.org/10.1128/AEM.02342-17.
37. Wang H, Zhang Y, Bartlett DH, Xiao X. 2021. Transcriptomic analysis reveals common adaptation mechanisms under different stresses for moderately piezophilic bacteria. Microb Ecol 81:617–629. https://doi.org/10.1007/s00248-020-01609-3.
38. Wang FP, Zhang Y, Chen Y, He Y, Qi J, Hinrichs KU, Zhang XX, Xiao X, Boon N. 2014. Methanotrophic archaea possessing diverging methane-oxidizing and electron-transporting pathways. ISME J 8:1069–1078. https://doi.org/10.1038/ismej.2013.212.
39. Santana M. 2008. Presence and expression of terminal oxygen reductases in strictly anaerobic sulfate-reducing bacteria isolated from salt-marsh sediments. Anaerobe 14:145–156. https://doi.org/10.1016/j.anaerobe.2008.03.001.
40. van Grinsven S, Sinninghe Damste JS, Abdala Asbun A, Engelmann JC, Harrison J, Villanueva L. 2020. Methane oxidation in anoxic lake water stimulated by nitrate and sulfate addition. Environ Microbiol 22:766–782. https://doi.org/10.1111/1462-2920.14886.
41. Blees J, Niemann H, Wenk CB, Zopfi J, Schubert CJ, Kirf MK, Veronesi ML, Hitz C, Lehmann MF. 2014. Micro-aerobic bacterial methane oxidation in the chemocline and anoxic water column of deep south-Alpine Lake Lugano (Switzerland). Limnol Oceanogr 59:311–324. https://doi.org/10.4319/lo.2014.59.2.0311.
42. Schubert CJ, Coolen MJL, Neretin LN, Schippers A, Abbas B, Durisch-Kaiser E, Wehrli B, Hopmans EC, Damsté JSS, Wakeham S, Kuypers MMM. 2006. Aerobic and anaerobic methanotrophs in the Black Sea water column. Environ Microbiol 8:1844–1856. https://doi.org/10.1111/j.1462-2920.2006.01079.x.
43. Cabrol L, Thalasso F, Gandois L, Sepulveda-Jauregui A, Martinez-Cruz K, Teisserenc R, Tananaev N, Tveit A, Svenning MM, Barret M. 2020. Anaerobic oxidation of methane and associated microbiome in anoxic water of Northwestern Siberian lakes. Sci Total Environ 736:139588. https://doi.org/10.1016/j.scitotenv.2020.139588.
44. Kalyuzhnaya MG, Yang S, Rozova ON, Smalley NE, Clubb J, Lamb A, Gowda GA, Raftery D, Fu Y, Bringel F, Vuilleumier S, Beck DA, Trotsenko YA, Khmelenina VN, Lidstrom ME. 2013. Highly efficient methane biocatalysis revealed in a methanotrophic bacterium. Nat Commun 4:2785. https://doi.org/10.1038/ncomms3785.
45. Padilla CC, Bertagnolli AD, Bristow LA, Sarode N, Glass JB, Thamdrup B, Stewart FJ. 7 February 2017. Metagenomic binning recovers a transcriptionally active gammaproteobacterium linking methanotrophy to partial denitrification in an anoxic oxygen minimum zone. Front Mar Sci https://doi.org/10.3389/fmars.2017.00023.
46. Kits KD, Klotz MG, Stein LY. 2015. Methane oxidation coupled to nitrate reduction under hypoxia by the Gammaproteobacterium Methylomonas denitrificans, sp. nov. type strain FJG1. Environ Microbiol 17:3219–3232. https://doi.org/10.1111/1462-2920.12772.
47. Milucka J, Kirf M, Lu L, Krupke A, Lam P, Littmann S, Kuypers MMM, Schubert CJ. 2015. Methane oxidation coupled to oxygenic photosynthesis in anoxic waters. ISME J 9:1991–2002. https://doi.org/10.1038/ismej.2015.12.
48. Mayr MJ, Zimmermann M, Guggenheim C, Brand A, Bürgmann H. 2020. Niche partitioning of methane-oxidizing bacteria along the oxygen–methane counter gradient of stratified lakes. ISME J 14:274–287. https://doi.org/10.1038/s41396-019-0515-8.
49. He R, Wang J, Pohlman JW, Jia Z, Chu Y-X, Wooller MJ, Leigh MB. 2022. Metabolic flexibility of aerobic methanotrophs under anoxic conditions in Arctic lake sediments. ISME J 16:78–90. https://doi.org/10.1038/s41396-021-01049-y.
50. Wegener G, Krukenberg V, Ruff SE, Kellermann MY, Knittel K. 2016. Metabolic capabilities of microorganisms involved in and associated with the anaerobic oxidation of methane. Front Microbiol 7:46. https://doi.org/10.3389/fmicb.2016.00046.
51. Meyerdierks A, Kube M, Kostadinov I, Teeling H, Glöckner FO, Reinhardt R, Amann R. 2010. Metagenome and mRNA expression analyses of anaerobic methanotrophic archaea of the ANME-1 group. Environ Microbiol 12:422–439. https://doi.org/10.1111/j.1462-2920.2009.02083.x.
52. Deusner C, Meyer V, Ferdelman TG. 2010. High-pressure systems for gas-phase free continuous incubation of enriched marine microbial communities performing anaerobic oxidation of methane. Biotechnol Bioeng 105:524–533. https://doi.org/10.1002/bit.22553.
53. Krüger M, Wolters H, Gehre M, Joye SB, Richnow H-H. 2008. Tracing the slow growth of anaerobic methane-oxidizing communities by 15N-labelling techniques. FEMS Microbiol Ecol 63:401–411. https://doi.org/10.1111/j.1574-6941.2007.00431.x.
54. Krüger M, Blumenberg M, Kasten S, Wieland A, Känel L, Klock J-H, Michaelis W, Seifert R. 2008. A novel, multi-layered methanotrophic microbial mat system growing on the sediment of the Black Sea. Environ Microbiol 10:1934–1947. https://doi.org/10.1111/j.1462-2920.2008.01607.x.

55. Timmers PHA, Gieteling J, Widjaja-Greefkes HCA, Plugge CM, Stams AJM, Lens PNL, Meulepas RJW. 2015. Growth of anaerobic methane-oxidizing archaea and sulfate-reducing bacteria in a high-pressure membrane capsule bioreactor. Appl Environ Microbiol 81:1286–1296. https://doi.org/10.1128/AEM.03255-14.
56. Cassarini C, Zhang Y, Lens PNL. 2019. Pressure selects dominant anaerobic methanotrophic phylotype and sulfate reducing bacteria in coastal marine Lake Grevelingen sediment. Front Environ Sci https://doi.org/10.3389/fenvs.2018.00162.
57. Zhuang G-C, Montgomery A, Joye SB. 2019. Heterotrophic metabolism of C1 and C2 low molecular weight compounds in northern Gulf of Mexico sediments: controlling factors and implications for organic carbon degradation. Geochim Cosmochim Acta 247:243–260. https://doi.org/10.1016/j.gca.2018.10.019.
58. Zhuang G-C, Heuer VB, Lazar CS, Goldhammer T, Wendt J, Samarkin VA, Elvert M, Teske AP, Joye SB, Hinrichs K-U. 2018. Relative importance of methylotrophic methanogenesis in sediments of the Western Mediterranean Sea. Geochim Cosmochim Acta 224:171–186. https://doi.org/10.1016/j.gca.2017.12.024.
59. Zhuang GC, Montgomery A, Sibert RJ, Rogener MK, Samarkin VA, Joye SB. 2018. Effects of pressure, methane concentration, sulfate reduction activity, and temperature on methane production in surface sediments of the Gulf of Mexico. Limnol Oceanogr 63:2080–2092. https://doi.org/10.1002/lno.10925.
60. Zhang Y, Maignien L, Zhao X, Wang F, Boon N. 2011. Enrichment of a microbial community performing anaerobic oxidation of methane in a continuous high-pressure bioreactor. BMC Microbiol 11:137. https://doi.org/10.1186/1471-2180-11-137.
61. Stams AJ, Plugge CM. 2009. Electron transfer in syntrophic communities of anaerobic bacteria and archaea. Nat Rev Microbiol 7:568–577. https://doi.org/10.1038/nrmicro2166.
62. Widdel F, Bak F. 1992. Gram-negative mesophilic sulfate-reducing bacteria, p 3352–3378. *In* Balows A, Trüper HG, Dworkin M, Harder W, Schleifer K-H (ed), The prokaryotes: a handbook on the biology of bacteria: ecophysiology, isolation, identification, applications. Springer New York, New York, NY.
63. Luff R, Wallmann K. 2003. Fluid flow, methane fluxes, carbonate precipitation and biogeochemical turnover in gas hydrate-bearing sediments at Hydrate Ridge, Cascadia Margin: numerical modeling and mass balances. Geochim Cosmochim Acta 67:3403–3421. https://doi.org/10.1016/S0016-7037(03)00127-3.
64. Natarajan VP, Zhang X, Morono Y, Inagaki F, Wang F. 2016. A modified SDS-based DNA extraction method for high quality environmental DNA from seafloor environments. Front Microbiol 7:986. https://doi.org/10.3389/fmicb.2016.00986.
65. Klindworth A, Pruesse E, Schweer T, Peplies J, Quast C, Horn M, Glockner FO. 2013. Evaluation of general 16S ribosomal RNA gene PCR primers for classical and next-generation sequencing-based diversity studies. Nucleic Acids Res 41:e1. https://doi.org/10.1093/nar/gks808.
66. Magoc T, Salzberg SL. 2011. FLASH: fast length adjustment of short reads to improve genome assemblies. Bioinformatics 27:2957–2963. https://doi.org/10.1093/bioinformatics/btr507.
67. Jorgensen SL, Hannisdal B, Lanzen A, Baumberger T, Flesland K, Fonseca R, Ovreas L, Steen IH, Thorseth IH, Pedersen RB, Schleper C. 2012. Correlating microbial community profiles with geochemical data in highly stratified sediments from the Arctic Mid-Ocean Ridge. Proc Natl Acad Sci U S A 109:E2846–E2855. https://doi.org/10.1073/pnas.1207574109.
68. Langille MG, Zaneveld J, Caporaso JG, McDonald D, Knights D, Reyes JA, Clemente JC, Burkepile DE, Vega Thurber RL, Knight R, Beiko RG, Huttenhower C. 2013. Predictive functional profiling of microbial communities using 16S rRNA marker gene sequences. Nat Biotechnol 31:814–821. https://doi.org/10.1038/nbt.2676.
69. Nurk S, Meleshko D, Korobeynikov A, Pevzner PA. 2017. metaSPAdes: a new versatile metagenomic assembler. Genome Res 27:824–834. https://doi.org/10.1101/gr.213959.116.
70. Li H, Handsaker B, Wysoker A, Fennell T, Ruan J, Homer N, Marth G, Abecasis G, Durbin R, Genome Project Data Processing Subgroup. 2009. The Sequence Alignment/Map format and SAMtools. Bioinformatics 25:2078–2079. https://doi.org/10.1093/bioinformatics/btp352.
71. Kang DD, Li F, Kirton E, Thomas A, Egan R, An H, Wang Z. 2019. MetaBAT 2: an adaptive binning algorithm for robust and efficient genome reconstruction from metagenome assemblies. PeerJ 7:e7359. https://doi.org/10.7717/peerj.7359.
72. Wu YW, Simmons BA, Singer SW. 2016. MaxBin 2.0: an automated binning algorithm to recover genomes from multiple metagenomic datasets. Bioinformatics 32:605–607. https://doi.org/10.1093/bioinformatics/btv638.
73. Alneberg J, Bjarnason BS, de Bruijn I, Schirmer M, Quick J, Ijaz UZ, Lahti L, Loman NJ, Andersson AF, Quince C. 2014. Binning metagenomic contigs by coverage and composition. Nat Methods 11:1144–1146. https://doi.org/10.1038/nmeth.3103.
74. Sieber CMK, Probst AJ, Sharrar A, Thomas BC, Hess M, Tringe SG, Banfield JF. 2018. Recovery of genomes from metagenomes via a dereplication, aggregation and scoring strategy. Nat Microbiol 3:836–843. https://doi.org/10.1038/s41564-018-0171-1.
75. Parks DH, Imelfort M, Skennerton CT, Hugenholtz P, Tyson GW. 2015. CheckM: assessing the quality of microbial genomes recovered from isolates, single cells, and metagenomes. Genome Res 25:1043–1055. https://doi.org/10.1101/gr.186072.114.
76. Chaumeil PA, Mussig AJ, Hugenholtz P, Parks DH. 2020. GTDB-Tk: a toolkit to classify genomes with the Genome Taxonomy Database. Bioinformatics 36:1925–1927. https://doi.org/10.1093/bioinformatics/btz848.
77. Hyatt D, Chen GL, Locascio PF, Land ML, Larimer FW, Hauser LJ. 2010. Prodigal: prokaryotic gene recognition and translation initiation site identification. BMC Bioinformatics 11:119. https://doi.org/10.1186/1471-2105-11-119.
78. Kanehisa M, Sato Y, Morishima K. 2016. BlastKOALA and GhostKOALA: KEGG tools for functional characterization of genome and metagenome sequences. J Mol Biol 428:726–731. https://doi.org/10.1016/j.jmb.2015.11.006.
79. Huerta-Cepas J, Szklarczyk D, Heller D, Hernandez-Plaza A, Forslund SK, Cook H, Mende DR, Letunic I, Rattei T, Jensen LJ, von Mering C, Bork P. 2019. eggNOG 5.0: a hierarchical, functionally and phylogenetically annotated orthology resource based on 5090 organisms and 2502 viruses. Nucleic Acids Res 47:D309–D314. https://doi.org/10.1093/nar/gky1085.
80. Huerta-Cepas J, Forslund K, Coelho LP, Szklarczyk D, Jensen LJ, von Mering C, Bork P. 2017. Fast genome-wide functional annotation through orthology assignment by eggNOG-Mapper. Mol Biol Evol 34:2115–2122. https://doi.org/10.1093/molbev/msx148.
81. Aramaki T, Blanc-Mathieu R, Endo H, Ohkubo K, Kanehisa M, Goto S, Ogata H. 2020. KofamKOALA: KEGG Ortholog assignment based on profile HMM and adaptive score threshold. Bioinformatics 36:2251–2252. https://doi.org/10.1093/bioinformatics/btz859.
82. Liao Y, Smyth GK, Shi W. 2014. featureCounts: an efficient general purpose program for assigning sequence reads to genomic features. Bioinformatics 30:923–930. https://doi.org/10.1093/bioinformatics/btt656.
83. Kultima JR, Sunagawa S, Li J, Chen W, Chen H, Mende DR, Arumugam M, Pan Q, Liu B, Qin J, Wang J, Bork P. 2012. MOCAT: a metagenomics assembly and gene prediction toolkit. PLoS One 7:e47656. https://doi.org/10.1371/journal.pone.0047656.
84. Yamada KD, Tomii K, Katoh K. 2016. Application of the MAFFT sequence alignment program to large data-reexamination of the usefulness of chained guide trees. Bioinformatics 32:3246–3251. https://doi.org/10.1093/bioinformatics/btw412.
85. Capella-Gutierrez S, Silla-Martinez JM, Gabaldon T. 2009. trimAl: a tool for automated alignment trimming in large-scale phylogenetic analyses. Bioinformatics 25:1972–1973. https://doi.org/10.1093/bioinformatics/btp348.
86. Nguyen LT, Schmidt HA, von Haeseler A, Minh BQ. 2015. IQ-TREE: a fast and effective stochastic algorithm for estimating maximum-likelihood phylogenies. Mol Biol Evol 32:268–274. https://doi.org/10.1093/molbev/msu300.
87. Parks DH, Beiko RG. 2010. Identifying biologically relevant differences between metagenomic communities. Bioinformatics 26:715–721. https://doi.org/10.1093/bioinformatics/btq041.
88. Kalvari I, Nawrocki EP, Ontiveros-Palacios N, Argasinska J, Lamkiewicz K, Marz M, Griffiths-Jones S, Toffano-Nioche C, Gautheret D, Weinberg Z, Rivas E, Eddy SR, Finn RD, Bateman A, Petrov AI. 2021. Rfam 14: expanded coverage of metagenomic, viral and microRNA families. Nucleic Acids Res 49:D192–D200. https://doi.org/10.1093/nar/gkaa1047.
89. Langmead B, Salzberg SL. 2012. Fast gapped-read alignment with Bowtie 2. Nat Methods 9:357–359. https://doi.org/10.1038/nmeth.1923.